PHYSICAL REVIEW MATERIALS **5**, 073609 (2021)

Elastic dipole tensor of a defect at a finite temperature: Definition and properties

Pui-Wai Ma[*] and S. L. Dudarev
UK Atomic Energy Authority, Culham Science Centre, Abingdon, Oxfordshire OX14 3DB, United Kingdom

(Received 16 April 2021; accepted 9 July 2021; published 30 July 2021)

The concept of the elastic dipole tensor of a defect is generalized to enable the treatment of lattice distortions produced by defects at elevated temperatures. Thermodynamic and statistical mechanics treatments show the feasibility of applying the formalism to the evaluation of formation free energies and finite-temperature elastic dipole tensors of $\frac{1}{2}\langle 111\rangle$ prismatic self-interstitial atom dislocation loops. The method exhibits good numerical stability even in the high-temperature limit, and relates discrete atomic and continuum representations of displacement and stress and strain fields of defects.

DOI: 10.1103/PhysRevMaterials.5.073609

I. INTRODUCTION

In a crystalline material, defects form spontaneously by thermal excitation. At thermal equilibrium, the concentration of defects is determined by their formation free energy and temperature. A high concentration of defects, far above the equilibrium value, can also be produced by mechanical deformation or by exposing materials to a flux of energetic particles [1–4].

There is an extensive variety of defects. Some of them can be readily classified and identified as a vacancy, a self-interstitial atom, a dislocation loop, a void, or an extended dislocation. Defects evolve under the effect of applied stress and temperature, segregating and agglomerating as a result of elastic interactions [5–7], or annihilate in reactions involving defects of opposite type. The evolution of microstructure driven by the generation of defects and reactions between them alters mechanical and physical properties of materials [8].

Defects distort the surrounding crystal lattice, producing spatially varying strain and stress fields. The strain field of a localized defect can be computed from its elastic dipole tensor and elastic Green's function [9–18], where the elastic dipole tensor is a fundamental quantity fully defining the elastic field of a defect in the asymptotic far-field limit [19]. Elements of the relaxation volume tensor and relaxation volumes of defects can also be computed using atomistic or *ab initio* methods [11–18,20,21].

The notion of an elastic dipole tensor transfers information, derived from discrete atomic configurations, to the continuum limit, and enables treating defects as objects of elasticity theory. This provides a foundation for continuum models of microstructural evolution and enables the evaluation of stress and strain fields on the spatial scale many orders of magnitude larger than that accessible to atomistic or electronic scale models [7,14,22].

The energy of elastic interaction between a defect and an external slowly spatially varying strain field $\epsilon_{ij}^{\text{ext}}$ can be written as

$$\mathcal{E}_{\text{int}}^{\text{ext}} = -P_{ij}\epsilon_{ij}^{\text{ext}}, \tag{1}$$

whereas the energy of elastic interaction between any two defects separated by a distance many times their size is

$$\mathcal{E}_{\text{int}}^{ab} = P_{ij}^{a}P_{kl}^{b}\frac{\partial^2}{\partial x_j \partial x_l}G_{ik}(\mathbf{r}), \tag{2}$$

where P_{ij}^{a} and P_{kl}^{b} are the dipole tensors of defects a and b, $\mathbf{r}$ is the relative position vector of the defects, and G_{ik} is the elastic Green's function. G_{ik} can be evaluated numerically for an arbitrary elastically anisotropic material [23] from its elastic constants tensor C_{ijkl}. In Eq. (2), summation over repeated indexes is assumed.

The pairwise nature of elastic interactions makes Eqs. (1) and (2) easily suitable for implementing in coarse-grained models, for example object kinetic Monte Carlo (kMC) [24–26] or defect dynamics [22]. Using the dipole tensor formalism, Sivak *et al.* estimated the effect of elastic interactions on the diffusion of defects in bcc iron and vanadium [24], as well as on the diffusion of hydrogen in bcc iron [25,26]. Baraglia *et al.* [22] used Eqs. (1) and (2) to simulate the time evolution of an ensemble of dislocation loops in tungsten.

A point that so far has not been extensively studied in the context of models using the elastic dipole tensor formalism is the role of temperature. All the calculations of dipole tensors of defects [15–17] were performed without considering thermal effects, despite the fact that applications always refer to observations or simulations performed at a finite temperature [22,24–26]. For example, it is the energy rather than the free energy that is often used in the analysis, and all the calculations of dipole tensors performed so far use molecular statics or density functional theory that involves the minimization of energy via ionic relaxation [15–18].

In this study, we extend the notion of the elastic dipole tensor to finite temperatures. We derive it from both the thermodynamics (macroscopic) and statistical mechanics (microscopic) perspectives using the free energy as the central notion of the theory of elasticity [27]. We find that the derivation leads to the same consistent result, provided that the Cauchy stress is taken as being equivalent to the ensemble

---

[*] leo.ma@ukaea.uk

average of the virial stress. We develop a numerical procedure for evaluating the formation free energy and elastic dipole tensor of defects, considering $\frac{1}{2}\langle 111\rangle$ self-interstitial atom (SIA) loops in tungsten as examples. We also discuss the effect of temperature on the free energy of elastic interaction between two isolated defects.

II. THEORY

At a finite temperature, the quantity used for evaluating the thermodynamic properties of a material is its free energy as opposed to energy. The free energy of an elastically strained crystalline solid equals [27]

$$\mathcal{F} = \frac{1}{2}\int \sigma_{ij}(\mathbf{r})\epsilon_{ij}(\mathbf{r})dV, \tag{3}$$

where $\sigma_{ij}(\mathbf{r})$ and $\epsilon_{ij}(\mathbf{r})$ are the spatially varying internal stress and strain, respectively. If the elastic stress and strain fields in the above equation are generated by the presence of a defect, the integral above gives its elastic free self-energy.

A small variation of the elastic field gives rise to a small variation in the free energy,

$$\begin{aligned}\mathcal{F} + \delta\mathcal{F} &= \frac{1}{2}\int \sigma_{ij}(\mathbf{r})\epsilon_{ij}(\mathbf{r})dV + \int \sigma_{ij}(\mathbf{r})\delta\epsilon_{ij}(\mathbf{r})dV \\ &= \frac{1}{2}\int \sigma_{ij}(\mathbf{r})\epsilon_{ij}(\mathbf{r})dV + \int \epsilon_{ij}(\mathbf{r})\delta\sigma_{ij}(\mathbf{r})dV,\end{aligned} \tag{4}$$

where the equivalence between the two forms of Eq. (4) stems from the quadratic form of Eq. (3) and the fact that $\sigma_{ij}(\mathbf{r}) = C_{ijkl}\epsilon_{kl}(\mathbf{r})$.

If the variation of strain is spatially homogeneous $\delta\epsilon_{ij}(\mathbf{r}) = \delta\epsilon_{ij}$, we write

$$\mathcal{F}(\delta\epsilon_{ij}) = \mathcal{F}(\delta\epsilon_{ij} = 0) + \left.\frac{\partial\mathcal{F}}{\partial\epsilon_{ij}}\right|_{\delta\epsilon_{ij}=0}\delta\epsilon_{ij}, \tag{5}$$

and hence

$$\mathcal{F}(\delta\epsilon_{ij}) = \mathcal{F}(\delta\epsilon_{ij} = 0) + \left[\int \sigma_{ij}(\mathbf{r})dV\right]\delta\epsilon_{ij}. \tag{6}$$

Differentiating the above equation with respect to strain, we find the dipole tensor of the defect, expressed as a volume integral of its stress field [11,12,19],

$$P_{ij} = \frac{\partial\mathcal{F}}{\partial\epsilon_{ij}} = \int \sigma_{ij}(\mathbf{r})dV = V\bar{\sigma}_{ij}. \tag{7}$$

The stress field here refers to its finite-temperature value [27]. Similarly, by differentiating the free energy with respect to a spatially homogeneous stress, we find the relaxation volume tensor of the defect [14,28] expressed as a volume integral of its strain field,

$$\Omega_{ij} = \frac{\partial\mathcal{F}}{\partial\sigma_{ij}} = \int \epsilon_{ij}(\mathbf{r})dV. \tag{8}$$

The two quantities (7) and (8) are related in the same way as elastic stress and strain, namely $P_{ij} = C_{ijkl}\Omega_{kl}$.

The free energy of interaction between a defect and a spatially homogeneous or slowly varying external field can now be readily derived from Eq. (4) using the fact that in equilibrium the variation of the stress field of the defect equals the applied external stress field taken with the opposite sign [19,27,29],

$$\mathcal{F}_{\text{int}}^{\text{ext}} = -\Omega_{ij}\sigma_{ij}^{\text{ext}} = -P_{ij}\epsilon_{ij}^{\text{ext}}. \tag{9}$$

In statistical mechanics, the free energy is related to the partition function of the system as

$$\mathcal{F} = -k_B T \ln \mathcal{Z}. \tag{10}$$

The partition function is

$$\mathcal{Z} = \int \exp(-\beta\mathcal{H})d\Omega, \tag{11}$$

where $\beta = (k_B T)^{-1}$ and $d\Omega$ refers to integration over phase space. Taking a functional derivative of the free energy with respect to internal strain gives

$$\frac{\delta\mathcal{F}}{\delta\epsilon_{ij}} = \frac{1}{\mathcal{Z}}\int \exp(-\beta\mathcal{H})\frac{\delta\mathcal{H}}{\delta\epsilon_{ij}}d\Omega = \left\langle\frac{\delta\mathcal{H}}{\delta\epsilon_{ij}}\right\rangle, \tag{12}$$

where brackets $\langle\ldots\rangle$ refer to the evaluation of an ensemble average quantity.

For an atomic system subjected to a small spatially homogeneous external strain, atomic position vectors transform in response to strain as

$$\mathbf{r} \to (\mathbf{I} + \boldsymbol{\epsilon}^{\text{ext}})\mathbf{r}. \tag{13}$$

Similarly, the momenta of atoms transform as

$$\mathbf{p} \to (\mathbf{I} + \boldsymbol{\epsilon}^{\text{ext}})^{-1}\mathbf{p}. \tag{14}$$

The above scaling of momentum is consistent with the definition of the momentum operator $\hat{\mathbf{p}} = -i\hbar\partial/\partial\mathbf{r}$ in quantum mechanics [30] or the Lagrangian classical mechanics [31], where the momentum is defined as a derivative of the Lagrangian function with respect to the corresponding velocity $\mathbf{p} = \partial\mathcal{L}/\partial\dot{\mathbf{r}}$. This results in

$$\left(\frac{\delta r_{n\alpha}}{\delta\epsilon_{ij}^{\text{ext}}}\right)_{\epsilon_{ij}^{\text{ext}}=0} = r_{nj}\delta_{\alpha i}, \tag{15}$$

$$\left(\frac{\delta p_{n\alpha}}{\delta\epsilon_{ij}^{\text{ext}}}\right)_{\epsilon_{ij}^{\text{ext}}=0} = -p_{nj}\delta_{\alpha i}, \tag{16}$$

where n refers to an atom and α is an index of a Cartesian coordinate.

Consider a generic atomic Hamiltonian of the form

$$\mathcal{H} = \sum_n \frac{\mathbf{p}_n^2}{2m} + U(\{\mathbf{r}\}), \tag{17}$$

where $U(\mathbf{r}_1, \mathbf{r}_2, \ldots, \mathbf{r}_N)$ is the potential energy, the value of which is uniquely defined by an atomic configuration $\{\mathbf{r}\} = (\mathbf{r}_1, \mathbf{r}_2, \ldots, \mathbf{r}_N)$. The functional derivative of the Hamiltonian with respect to an external strain is

$$\frac{\delta\mathcal{H}}{\delta\epsilon_{ij}^{\text{ext}}} = \sum_{n,\alpha}\frac{p_{n\alpha}}{m}\left(\frac{\delta p_{n\alpha}}{\delta\epsilon_{ij}^{\text{ext}}}\right) + \sum_{n,\alpha}\frac{\partial U}{\partial r_{n\alpha}}\left(\frac{\delta r_{n\alpha}}{\delta\epsilon_{ij}^{\text{ext}}}\right) \tag{18}$$

$$= -\sum_n \frac{p_{ni}p_{nj}}{m} - \sum_n F_{ni}r_{nj} \tag{19}$$

$$= -\sum_n \frac{p_{ni}p_{nj}}{m} + \frac{1}{2}\sum_{nm}F_{nmi}(r_{mj} - r_{nj}) \tag{20}$$

$$= V\bar{\sigma}_{ij}^{\text{vir}}, \tag{21}$$

where $F_{ni} = -\partial U/\partial r_{ni}$ is the ith Cartesian component of the force acting on atom n, F_{nmi} is the ith component of the force acting on atom n due to its interaction with atom m, and V is the volume of the system. The virial stress in an atomic system is defined as [32,33],

$$\bar{\sigma}_{ij}^{\rm vir} = \frac{1}{V}\left(-\sum_{n}\frac{p_{ni}p_{nj}}{m} + \frac{1}{2}\sum_{m,n}F_{nmi}(r_{mj} - r_{nj})\right). \tag{22}$$

Therefore, we can write

$$\frac{\delta\mathcal{H}}{\delta\epsilon_{ij}} = -\frac{\delta\mathcal{H}}{\delta\epsilon_{ij}^{\rm ext}} = -V\bar{\sigma}_{ij}^{\rm vir}. \tag{23}$$

The sign convention for the virial stress is that $P = -\frac{1}{3}{\rm Tr}(\bar{\boldsymbol{\sigma}}^{\rm vir})$, where P is the external hydrostatic pressure. In equilibrium, the sign of the virial stress is opposite to that of the internal stress. Finally, we arrive at [cf. Eq. (7)]

$$\frac{\delta\mathcal{F}}{\delta\epsilon_{ij}} = \left\langle\frac{\delta\mathcal{H}}{\delta\epsilon_{ij}}\right\rangle = -V\langle\bar{\sigma}_{ij}^{\rm vir}\rangle = V\langle\bar{\sigma}_{ij}\rangle, \tag{24}$$

where $\bar{\sigma}_{ij}$ is the average internal stress. The last equality holds following the same argument as that given in Ref. [14], where a defect in a simulation cell with a finite size is treated using periodic boundary conditions. The elastic dipole tensor, derived using a microscopic argument, can now be written as

$$P_{ij} = V\langle\bar{\sigma}_{ij}\rangle. \tag{25}$$

This expression has a form similar to that derived from the energy argument at 0 K [11–18]. However, now the formula also includes averaging over the statistical ensemble of realizations of the system. Furthermore, we find that the expression for the elastic dipole tensor in the macroscopic thermodynamics given by Eq. (7) is equivalent to that derived from the microscopic argument of statistical mechanics, provided that the Cauchy stress is taken as equivalent to the ensemble average value of the virial stress. The Cauchy stress and virial stress are equivalent in the thermodynamic limit [32].

In the 0 K limit, the dipole tensor can also be evaluated using the applied strain approach [11–13], which focuses on the difference between the simulation cell shape and volume with and without a defect, assuming stress-free conditions. This is because elastic strain and stress are related by the fourth-rank elastic constant tensor, according to linear elasticity [27]. In finite-temperature dynamic simulations, if a simulation cell is allowed to change its dimensions, it will not converge to a unique box shape and volume, because stress is a time-dependent fluctuating quantity. One needs to introduce at least one extra parameter to control the rate of variation of cell dimensions, which can cause bias in averaging. As a technical note, it is hard to apply the umbrella sampling method, which we will discuss in the next section. Our approach takes noninteracting harmonic oscillators as a reference. Since using a harmonic oscillator requires defining its equilibrium position at a certain location, we cannot use it as a reference if the dimensions of the simulation cell vary. In this study, we perform simulations with fixed dimensions of the simulation cell that are more suitable for practical implementation.

III. UMBRELLA SAMPLING

The nonstationary nature of a defect presents a difficulty in the context of evaluation of its thermodynamic properties, since a defect migrates and evolves due to the effect of thermal fluctuations. We circumvent this problem using a biased sampling technique known as the umbrella sampling [34]. It is a reweighting technique for evaluating a thermodynamic quantity of a target state by sampling a reference state. We briefly outline the method here, and then apply it specifically to the case of a defect at a finite temperature. We note that the method only applies in the classical limit, and it does not treat the low-temperature case where quantum-mechanical effects dominate the properties and dynamics of defects [35,36].

We consider two classical Hamiltonians $\mathcal{H}^0$ and $\mathcal{H}^1$, and their difference:

$$\delta\mathcal{H}_{\rm um} = \mathcal{H}^1 - \mathcal{H}^0. \tag{26}$$

The ensemble average of an observable $\mathcal{O}$ with respect to Hamiltonian $\mathcal{H}^0$ at temperature T is

$$\langle\mathcal{O}\rangle_0 = \frac{\int\mathcal{O}\exp(-\beta\mathcal{H}^0)d\Omega}{\int\exp(-\beta\mathcal{H}^0)d\Omega}. \tag{27}$$

Substituting Eq. (26) into (27), we find

$$\langle\mathcal{O}\rangle_0 = \frac{\langle\mathcal{O}\exp(\beta\delta\mathcal{H}_{\rm um})\rangle_1}{\langle\exp(\beta\delta\mathcal{H}_{\rm um})\rangle_1}. \tag{28}$$

This formula replaces the calculation of an average of an observable $\mathcal{O}$ over an ensemble defined by Hamiltonian $\mathcal{H}^0$ by calculations of averages of $\mathcal{O}\exp(\beta\delta\mathcal{H}_{\rm um})$ and $\exp(\beta\delta\mathcal{H}_{\rm um})$ over an ensemble defined by another Hamiltonian $\mathcal{H}^1$. In a dynamic simulation, an ensemble average quantity is calculated by taking a time average and assuming ergodicity. The values of $\mathcal{O}$ and $\delta\mathcal{H}_{\rm um}$ are calculated from the instantaneous momenta and positions of atoms.

We apply the above formula to the calculation of the elastic dipole tensor of a defect. The functional derivative of the free energy of a system defined by Hamiltonian $\mathcal{H}^0$ is

$$\frac{\delta\mathcal{F}^0}{\delta\epsilon_{ij}} = \frac{1}{\mathcal{Z}^0}\int\exp(-\beta\mathcal{H}^0)\frac{\delta\mathcal{H}^0}{\delta\epsilon_{ij}}d\Omega. \tag{29}$$

Combining this with Eq. (26), we arrive at

$$\frac{\delta\mathcal{F}^0}{\delta\epsilon_{ij}} = \frac{\int\exp(-\beta\mathcal{H}^1)\exp(\beta\delta H_{\rm um})\frac{\delta\mathcal{H}^0}{\delta\epsilon_{ij}}d\Omega}{\int\exp(-\beta\mathcal{H}^1)\exp(\beta\delta H_{\rm um})d\Omega}. \tag{30}$$

Multiplying this by $1 = \mathcal{Z}^1/\mathcal{Z}^1$, we transform the above equation into

$$\frac{\delta\mathcal{F}^0}{\delta\epsilon_{ij}} = \frac{\left\langle\frac{\delta\mathcal{H}^0}{\delta\epsilon_{ij}}\exp(\beta\delta\mathcal{H}_{\rm um})\right\rangle_1}{\langle\exp(\beta\delta\mathcal{H}_{\rm um})\rangle_1}. \tag{31}$$

The right-hand side of this equation is consistent with Eq. (28), showing that the derivative of the free energy and hence the dipole tensor of a defect can be evaluated using the umbrella sampling approach.

In addition to providing a way of evaluating observables, the umbrella sampling method also suggests a way of cal-

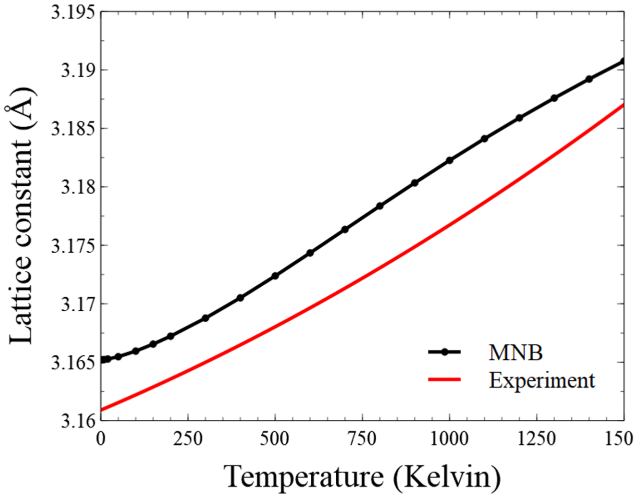

FIG. 1. Equilibrium lattice constants, calculated using the Mason–Nguyen-Manh–Becquart (MNB) [40] tungsten interatomic potential over a range of elevated temperatures. Experimental curve is given by a fitted formula taken from Ref. [41], where the measurements span the range from 25 to 900 °C.

culating the free energy. The free energy corresponding to Hamiltonian $\mathcal{H}^0$ can be written as

$$\mathcal{F}^0 = -k_B T \ln Z^0 \tag{32}$$

$$= -k_B T \ln \int \exp(-\beta \mathcal{H}^0) d\Omega. \tag{33}$$

Using Eq. (26), we find the free energy as

$$\mathcal{F}^0 = -k_B T \ln \int \exp(\beta \delta \mathcal{H}_{\mathrm{um}}) \exp(-\beta \mathcal{H}^1) d\Omega \tag{34}$$

$$= -k_B T \ln \langle \exp(\beta \delta \mathcal{H}_{\mathrm{um}}) \rangle_1 + \mathcal{F}^1. \tag{35}$$

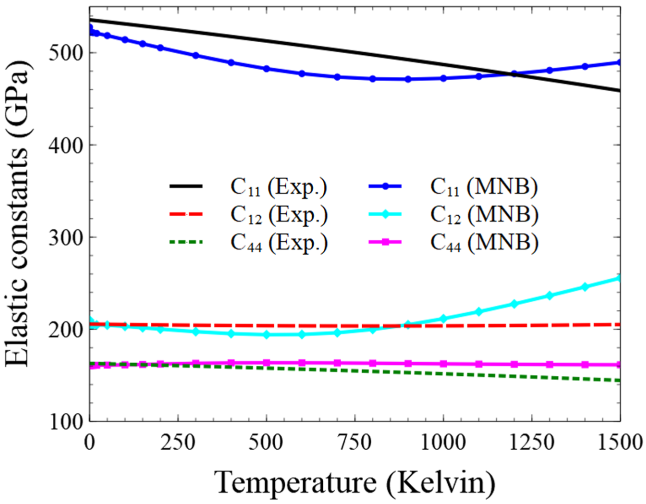

FIG. 2. Elastic constants C_{11}, C_{12}, and C_{44} evaluated from the free energy computed using the MNB potential for tungsten. Experimental data are taken from Ref. [42], where the measurements span the temperature range up to 1800 °C.

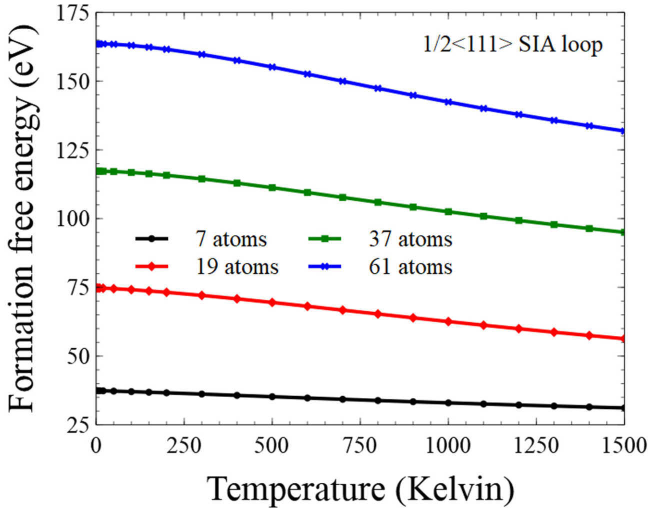

FIG. 3. Formation free energies of hexagonal $\frac{1}{2}\langle 111 \rangle$ SIA loops containing 7, 19, 37, and 61 extra atoms.

This shows that the free energy $\mathcal{F}^0$ can be evaluated by sampling over an ensemble defined by Hamiltonian $\mathcal{H}^1$ if $\mathcal{F}^1$ is known.

In practice, assuming that the system of interest involves N atoms, we choose Hamiltonian $\mathcal{H}^1$ as a sum of N three-dimensional noninteracting harmonic oscillators

$$\mathcal{H}^1 = \mathcal{H}_{HO} = \sum_n \left(\frac{\mathbf{p}_n^2}{2m} + \frac{1}{2} m\omega^2 \mathbf{x}_n^2 + C \right), \tag{36}$$

where $\mathbf{x}_n = \mathbf{r}_n - \mathbf{R}_n$ is the coordinate of an oscillator, defined near an equilibrium atomic position $\mathbf{R}_n$, ω is its frequency and m its mass, and C is a constant. The free energy of this system of oscillators, in the classical limit, can be evaluated analytically as [37]

$$\mathcal{F}^1 = \mathcal{F}_{HO} = -3Nk_B T \ln \left(\frac{k_B T}{\hbar\omega} \right) + NC, \tag{37}$$

where the Planck constant is included for dimensional convenience. In what follows, we assume that ω equals the Debye frequency of tungsten, $\hbar\omega = k_B T_D$, where $T_D = 400$ K. The choice of ω here is a matter of numerical convenience, and is consistent with that our case studies use the tungsten many-body potential. It by no means represents a constraint or limits the range of applications of the approach. Constant C is adjusted on the fly during the thermalization of a system, but remains fixed during sampling in order to minimize $\delta\mathcal{H}_{\mathrm{um}}$ and achieve higher accuracy of the final result. The initial atomic configuration containing a defect $\{\mathbf{R}_n\}$ is determined through energy minimization via atomic relaxation performed using the conjugate gradient method. The actual sampling is performed using molecular dynamic simulations, integrating the corresponding Langevin equations of motion [38].

IV. SIMULATIONS

Simulations exploring finite-temperature properties of defects were performed for $\frac{1}{2}\langle 111 \rangle$ SIA loops of various size in tungsten. We computed the formation free energies and elastic dipole tensors of loops at finite temperatures. All the

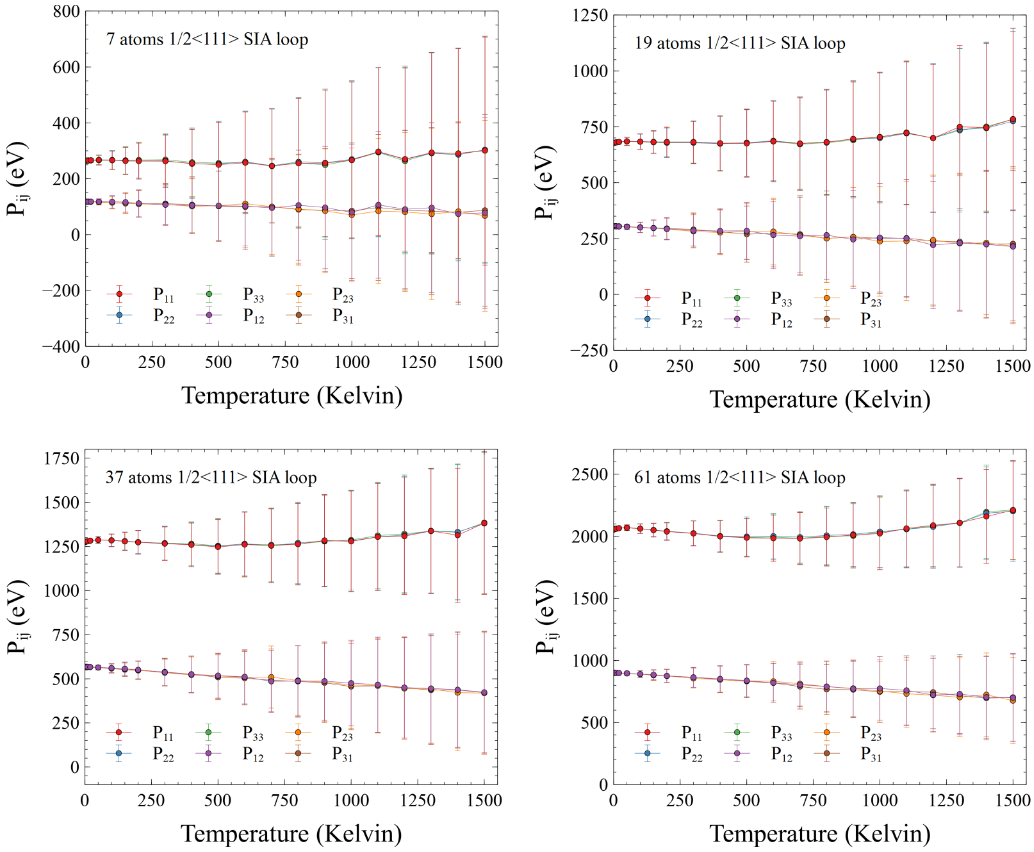

FIG. 4. Elastic dipole tensors of $\frac{1}{2}\langle 111\rangle$ self-interstitial atom dislocation loops containing 7, 19, 37, and 61 extra atoms calculated using the umbrella sampling according to Eq. (31). Standard deviations of data points are shown as error bars.

simulations were performed using the SPILADY spin-lattice dynamics code [39] modified to include the methodology described in this study.

The initial analysis was performed using simulation cells containing $30 \times 30 \times 30$ bcc cubic unit cells and 54 000 atoms. Each bcc cubic unit cell involves two atoms. We used the Mason–Nguyen-Manh–Becquart (MNB) [40] interatomic potential for tungsten. Simulation cells were thermalized to temperatures in the range from from 0.1 K to 1500 K. The volume of the cell was controlled by a barostat keeping the pressure fluctuating around 0 GPa. Following full thermalization, the average of cell dimensions was monitored over 2 ns to compute the equilibrium lattice constants. The results are shown in Fig. 1.

Using the equilibrium lattice constants computed for various temperatures, we explored the simulation cells with fixed shape, size, and volume containing $30 \times 30 \times 30$ unit cells. We evaluated the free energy of a perfect lattice using simulations involving 200 000 time steps. Then, we created six deformed boxes with uniaxial strains of $\pm 0.1\%$ in the x direction, biaxial strains of $\pm 0.05\%$ in both x and y directions, or shear strains of $\pm 0.1\%$ in the xy direction. By calculating the free energies and comparing them with the perfect lattice values, and using the expression for the elastic free energy

$$\mathcal{F} = \mathcal{F}_0 + \frac{V}{2} C_{ijkl}\epsilon_{ij}\epsilon_{kl}, \tag{38}$$

we determined the elastic constants C_{11}, C_{12}, and C_{44} in the Voigt notations. The resulting values of elastic constants are shown in Fig. 2. The experimentally measured elastic constants of tungsten, plotted using the fitted functions parametrized by Lowrie *et al.* [42], are also shown for comparison. The range of experimental data extends to 1800 °C.

Hexagonal or nearly circular $\frac{1}{2}\langle 111\rangle$ self-interstitial atom (SIA) dislocation loops containing 7, 19, 37, and 61 atoms were created in the initially perfect $30 \times 30 \times 30$ simulation cells. Atomic positions were determined by energy minimization through atomic relaxation performed using the conjugate gradient method, while constraining the shape and volume of the simulation cell. We evaluated the free energies of loops using the umbrella sampling and 200 000 integration time steps. The formation free energy was computed using the equation

$$\mathcal{F}^{\text{form}} = \mathcal{F}^{\text{def}} - \frac{N^{\text{def}}}{N^{\text{perf}}}\mathcal{F}^{\text{perf}}, \tag{39}$$

where $\mathcal{F}^{\text{def}}$ and $\mathcal{F}^{\text{perf}}$ are the free energies of configurations containing a defect and that of a perfect crystal, and N^{def} and N^{perf} are the numbers of atoms in the corresponding simulation cells. From Fig. 3 we see that all the formation free energies decrease monotonically as a function of temperature. The data also suggest that the rate of variation of the free energy as a function of temperature is greater for the larger loops.

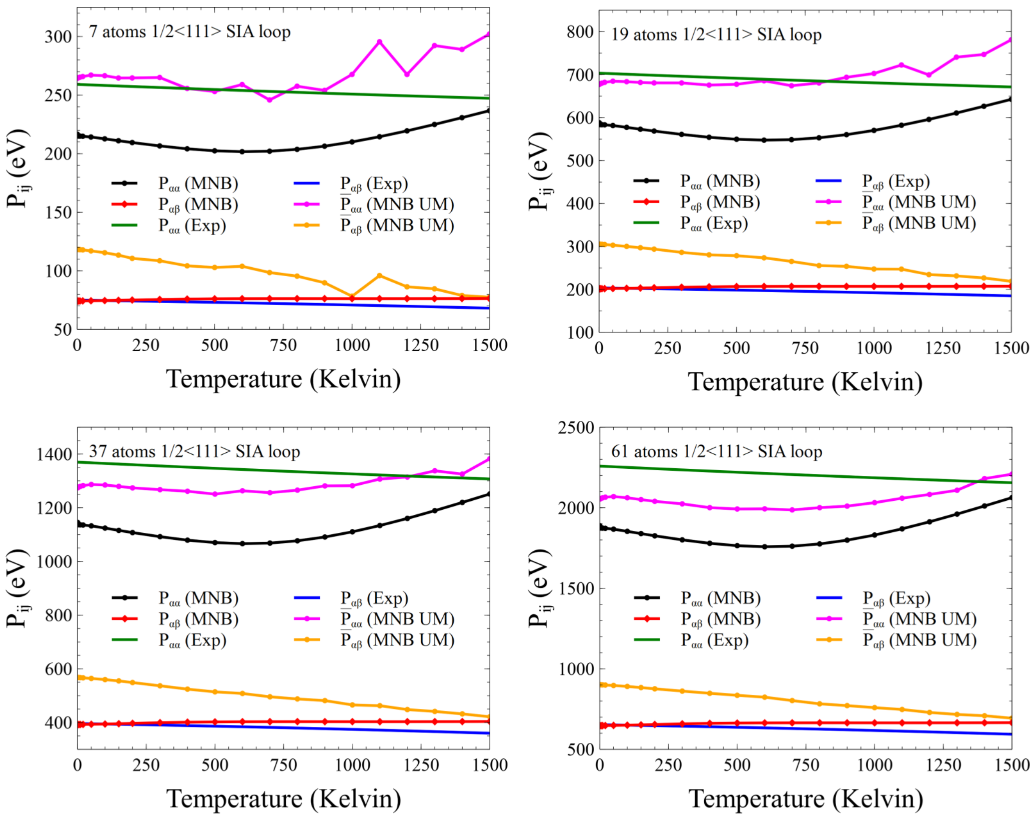

FIG. 5. Elastic dipole tensors of $\frac{1}{2}\langle 111\rangle$ SIA loops, containing 7, 19, 37, and 61 extra atoms, evaluated using Eq. (41) in the linear elasticity approximation. Temperature-dependent elastic constants and lattice constants are taken from experiments [41,42], and calculations are performed using the MNB potential. $P_{\alpha\alpha}$ are the diagonal elements and $P_{\alpha\beta}$ are the off-diagonal elements of the dipole tensor. Average values of the diagonal $\bar{P}_{\alpha\alpha} = (P_{11} + P_{22} + P_{33})/3$ and off-diagonal $\bar{P}_{\alpha\beta} = (P_{12} + P_{23} + P_{31})/3$ elements calculated using the umbrella sampling are presented for comparison.

There are other methods for computing the free energy, for example the local harmonic approximation [43], where the free energy is evaluated from the vibration frequencies determined by diagonalizing the dynamic matrix. This effectively maps a system of interacting atoms onto a system of independent harmonic oscillators with the same number of degrees of freedom. Thermodynamic integration [44,45] is another popular choice. However, in a calculation of the free energy of a defect, one needs to guarantee that the two integration end points are stable or at least metastable configurations. For a mobile SIA-type defect, it is hard to confine a defect configuration without imposing any constraint and treat it as a stable end point. On the other hand, umbrella sampling allows one to choose harmonic oscillators as the reference state, and this effectively holds the defect configuration. The umbrella sampling is a feasible way of evaluating the free energy, which appears efficient and suitable for a variety of applications [38]. Besides, the formalism of umbrella sampling enables achieving two objectives at the same time. In addition to evaluating the free energy, it also enables calculating various observables through reweighting.

An evaluation of a finite-temperature elastic dipole tensor involves an element of subtlety. Larger simulation cells containing $50 \times 50 \times 50$ unit cells are used, and the time integration involves 500 000 steps. The use of larger cell size offers an advantage by moderating fluctuations of the sum of atomic stresses. Furthermore, instead of using $\mathcal{H}^1 = \mathcal{H}_{HO}$, we choose

$$\mathcal{H}^1 = (1 - \lambda)\mathcal{H}_l + \lambda\mathcal{H}_{HO}, \tag{40}$$

where $\mathcal{H}_l$ is a generic lattice Hamiltonian [Eq. (17)] and $\lambda = 1 \times 10^{-7}$ is a small constant factor. The elastic dipole tensor of a loop is calculated using Eq. (31). In the calculation of an observable, it is not a requirement to use an analytically solvable reference state. The choice of a reference state can be different when a free energy calculation or a calculation of an observable is performed. There is no requirement that a unique reference state must always be used. The reason for adopting the numerical procedure above is to aim at choosing a small value of $\delta\mathcal{H}_{\mathrm{um}}$. If $\delta\mathcal{H}_{\mathrm{um}}$ is large, the exponential factor in Eq. (28) is also large, leading to large numerical errors. Besides, choosing a Hamiltonian $\mathcal{H}^1$ that is close to $\mathcal{H}^0$ implies that the phase space explored by the simulations is close to that of the original Hamiltonian, helping better quality sampling. The introduction of $\mathcal{H}_{HO}$ serves as the means for pinning the defect configuration.

Figure 4 shows how the elements of elastic dipole tensors of $\frac{1}{2}\langle 111\rangle$ SIA loops vary as functions of temperature for various loop sizes. Standard deviations of data are indicated by error bars. The magnitude of the standard deviation becomes larger at higher temperatures. Their values are almost the same in all four cases, because stress fluctuations are a consequence of thermal excitations. The mean values are not smooth when the loop size is small, because the error is relatively large.

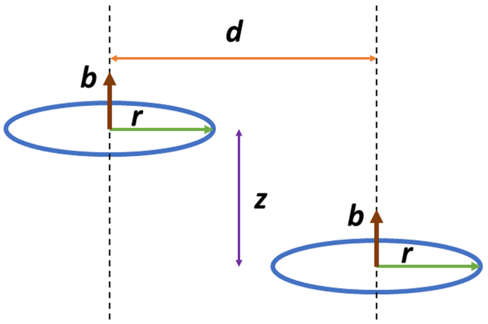

FIG. 6. Two pure prismatic dislocation loops with Burgers vectors $\mathbf{b} = \frac{a}{2}\langle 111\rangle$ and same radii r, where a is the bcc lattice parameter. Centers of the loops are separated horizontally by d and vertically by z.

There is an analytical expression for P_{ij} of a dislocation loop derived in the linear elasticity approximation [9,14,29,46,47]:

$$P_{ij} = C_{ijkl} b_k A_l, \tag{41}$$

where b_k and A_l are the Cartesian components of the Burgers vector $\mathbf{b}$ and the loop area vector $\mathbf{A}$. The loop area vector satisfies the condition $V = N\Omega_0 = \mathbf{b} \cdot \mathbf{A}$ [14], where N is the number of atoms forming the dislocation loop.

Using Eq. (41) we can evaluate the elastic dipole tensor of a loop from the finite-temperature values of elastic constants and lattice constants derived from experiment [41,42] and numerical simulations using the MNB potential performed in this study. Figure 5 shows values of the matrix elements of the dipole tensor computed in this way, where $P_{\alpha\alpha}$ are the diagonal elements and $P_{\alpha\beta}$ are the off-diagonal elements. For comparison, we also plot the average values of diagonal $\bar{P}_{\alpha\alpha} = (P_{11} + P_{22} + P_{33})/3$ and off-diagonal $\bar{P}_{\alpha\beta} = (P_{12} + P_{23} + P_{31})/3$ elements shown in Fig. 5.

We see that the values calculated according to linear elasticity are fairly similar to those derived from direct numerical calculations using the umbrella sampling. We note that the linear elasticity approximation ignores the dislocation core effects, which are more significant in the limit where a dislocation loop is small. According to the calculated and predicted values of P_{ij} of loops, we see that it is reasonable to use Eq. (41) derived from the continuum linear elasticity model, where the elastic constants are treated as temperature-dependent quantities.

Given that we can now evaluate the elastic dipole tensor of a loop at a finite temperature, what are the implications for the elastic interaction free energy? The free energy of elastic interaction between two defects can be written as

$$\mathcal{F}(\mathbf{r}) = P^a_{ij} P^b_{kl} G_{ik,jl}(\mathbf{r}). \tag{42}$$

Assuming the validity of linear elasticity, we illustrate the temperature effect by looking at loop-loop interactions. We place two pure prismatic loops with parallel Burgers vectors $\mathbf{b} = \frac{1}{2}\langle 111\rangle$ and radii $r = 2$ nm in a crystal as illustrated in Fig. 6. The loops are separated horizontally by a distance $d = 10$ nm and vertically by z. Using Eq. (41) and knowing that $G_{ik,jl}$ is also a function of C_{ijkl} [23], we can evaluate the elastic interaction free energy $\mathcal{F}$ using the temperature-dependent elastic constants derived from experiment [42].

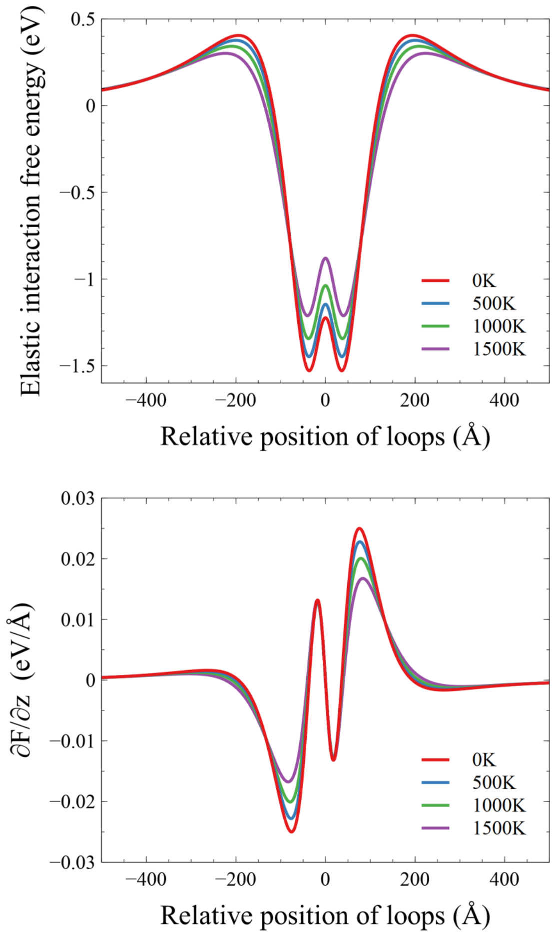

FIG. 7. Elastic interaction free energy (top) and variation of the free energy with respect to the relative vertical position z of two loops as shown in Fig. 6, where $r = 2$ nm and $d = 10$ nm (bottom), as a function of the relative vertical position z.

In Fig. 7, we plotted $\mathcal{F}$ and its derivative with respect to the relative vertical position $\partial\mathcal{F}/\partial z$ at various temperatures. The depth of the free energy well is responsible for the correlated motion of loops and $\partial\mathcal{F}/\partial z$ is the force acting on the loops [6]. As temperature increases, the free energy well becomes shallower, and the driving force that traps the loops at around ±75 Å weakens. In this example, we observe that the elastic dipole tensors of the loops vary as functions of temperature, the elastic Green's function varies because of its dependence on elastic constants, and the elastic interaction free energy varies as a function of temperature. In this particular example of loop-loop interaction, when the temperature increases the interaction weakens, implying that the two loops trapped by their mutual elastic interaction and undergoing correlated motion have a higher chance of being decoupled by random thermal fluctuations.

V. CONCLUSION

We extended the concept of the elastic dipole tensor to the treatment of the elastic field of a defect at a finite temperature.

The elastic dipole tensor is given by the volume integral of the stress field of a defect, like in the 0 K case; however now the calculation requires taking the ensemble average of the integral. Examples of $\frac{1}{2}\langle 111\rangle$ SIA loops illustrate the feasibility of carrying out calculations of formation free energies and elastic dipole tensors of defects at a finite temperature. We also find that the linear elasticity formulas for the dipole tensor of loops agree well with direct numerical simulations, enabling application of finite-temperature analysis to the continuum level simulations. A case study involving two interacting dislocation loops at finite temperature illustrates the effect of temperature on the free energy of elastic interaction, showing that the elastic interaction between the loops becomes weaker at higher temperatures.

Further information on the data and models underlying the paper is available [48].

ACKNOWLEDGMENTS

This work has been carried out within the framework of the EUROfusion Consortium and has received funding from the Euratom Research and Training Programme 2014–2018 and 2019–2020 under Grant Agreement No. 633053 and from the RCUK Energy Programme (Grant No. EP/T012250/1). The views and opinions expressed herein do not necessarily reflect those of the European Commission. We acknowledge the use of computer resources provided by the IRIS(STFC) Consortium.

[1] W. Cai and W. D. Nix, *Imperfections in Crystalline Solids* (Cambridge University Press, Cambridge, 2016).

[2] A. E. Sand, K. Nordlund, and S. L. Dudarev, Radiation damage production in massive cascades initiated by fusion neutrons in tungsten, J. Nucl. Mater. **455**, 207 (2014).

[3] A. E. Sand, M. J. Aliaga, M. J. Caturla, and K. Nordlund, Surface effects and statistical laws of defects in primary radiation damage: Tungsten vs. iron, Europhys. Lett. **115**, 36001 (2016).

[4] J. Byggmästar, F. Granberg, A. E. Sand, A. Pirttikoski, R. Alexander, M.-C. Marinica, and K. Nordlund, Collision cascades overlapping with self-interstitial defect clusters in Fe and W, J. Phys.: Condens. Matter **31**, 245402 (2019).

[5] A. D. Brailsford and R. Bullough, The theory of sink strengths, Philos. Trans. R. Soc., A **302**, 87 (1981).

[6] S. L. Dudarev, M. R. Gilbert, K. Arakawa, H. Mori, Z. Yao, M. L. Jenkins, and P. M. Derlet, Langevin model for real-time Brownian dynamics of interacting nanodefects in irradiated metals, Phys. Rev. B **81**, 224107 (2010).

[7] S. L. Dudarev, D. R. Mason, E. Tarleton, P.-W. Ma, and A. E. Sand, A multi-scale model for stresses, strains and swelling of reactor components under irradiation, Nucl. Fusion **58**, 126002 (2018).

[8] M. Durrand-Charre, *Microstructure of Steels and Cast Irons* (Springer-Verlag, Berlin, 2003).

[9] P. Dederichs, C. Lehmann, H. Schober, A. Scholz, and R. Zeller, Lattice theory of point defects, J. Nucl. Mater. **69-70**, 176 (1978).

[10] W. Schilling, Self-interstitial atoms in metals, J. Nucl. Mater. **69-70**, 465 (1978).

[11] E. Clouet, S. Garruchet, H. Nguyen, M. Perez, and C. S. Becquart, Dislocation interaction with C in α-Fe: A comparison between atomic simulations and elasticity theory, Acta Mater. **56**, 3450 (2008).

[12] C. Varvenne, F. Bruneval, M.-C. Marinica, and E. Clouet, Point defect modeling in materials: Coupling *ab initio* and elasticity approaches, Phys. Rev. B **88**, 134102 (2013).

[13] C. Varvenne and E. Clouet, Elastic dipoles of point defects from atomistic simulations, Phys. Rev. B **96**, 224103 (2017).

[14] S. L. Dudarev and P.-W. Ma, Elastic fields, dipole tensors, and interaction between self-interstitial atom defects in bcc transition metals, Phys. Rev. Mater. **2**, 033602 (2018).

[15] P.-W. Ma and S. L. Dudarev, Universality of point defect structure in body-centered cubic metals, Phys. Rev. Mater. **3**, 013605 (2019).

[16] P.-W. Ma and S. L. Dudarev, Symmetry-broken self-interstitial defects in chromium, molybdenum, and tungsten, Phys. Rev. Mater. **3**, 043606 (2019).

[17] P.-W. Ma and S. L. Dudarev, Effect of stress on vacancy formation and migration in body-centered-cubic metals, Phys. Rev. Mater. **3**, 063601 (2019).

[18] P.-W. Ma and S. L. Dudarev, CALANIE: Anisotropic elastic correction to the total energy, to mitigate the effect of periodic boundary conditions, Comput. Phys. Commun. **252**, 107130 (2019).

[19] G. Leibfried and N. Breuer, *Point Defects in Metals* (Springer, Berlin, 1978), p. 161.

[20] C. Domain and C. S. Becquart, *Ab initio* calculations of defects in Fe and dilute Fe–Cu alloys, Phys. Rev. B **65**, 024103 (2001).

[21] D. R. Mason, D. Nguyen-Manh, M.-C. Marinica, R. Alexander, A. E. Sand, and S. L. Dudarev, Relaxation volumes of microscopic and mesoscopic irradiation-induced defects in tungsten, J. Appl. Phys. **126**, 075112 (2019).

[22] F. Baraglia and P.-W. Ma, Dynamic model for an ensemble of interacting irradiation-induced defects in a macroscopic sample, Modell. Simul. Mater. Sci. Eng. **29**, 025004 (2021).

[23] D. M. Barnett, The precise evaluation of derivatives of the anisotropic elastic Green's functions, Phys. Status Solidi (b) **49**, 741 (1972).

[24] A. Sivak, V. Chernov, V. Romanov, and P. Sivak, Kinetic Monte-Carlo simulation of self-point defect diffusion in dislocation elastic fields in bcc iron and vanadium, J. Nucl. Mater. **417**, 1067 (2011).

[25] A. Sivak, P. Sivak, V. Romanov, and V. Chernov, Energetic, crystallographic and diffusion characteristics of hydrogen isotopes in iron, J. Nucl. Mater. **461**, 308 (2015).

[26] A. B. Sivak, P. A. Sivak, V. A. Romanov, and V. M. Chernov, Hydrogen diffusion in the elastic fields of dislocations in iron, Phys. At. Nucl. **79**, 1199 (2016).

[27] L. D. Landau and E. M. Lifshitz, *Theory of Elasticity*, 2nd ed. (Pergamon Press, Oxford, 1970).

[28] B. Puchala, M. L. Falk, and K. Garikipati, Elastic effects on relaxation volume tensor calculations, Phys. Rev. B **77**, 174116 (2008).

[29] A. P. Sutton, *Physics of Elasticity and Crystal Defects* (Oxford University Press, Oxford, 2020).

[30] L. D. Landau and E. M. Lifshitz, *Quantum Mechanics, Nonrelativistic Theory*, 2nd ed. (Pergamon Press, Oxford, 1965).

[31] L. D. Landau and E. M. Lifshitz, *Mechanics*, 3rd ed. (Butterworth-Heinemann, Oxford, 1976), p. 16.

[32] D. H. Tsai, The virial theorem and stress calculation in molecular dynamics, J. Chem. Phys. **70**, 1375 (1979).

[33] R. J. Swenson, Comments on virial theorems for bounded systems, Am. J. Phys. **51**, 940 (1983).

[34] G. Torrie and J. Valleau, Nonphysical sampling distributions in Monte Carlo free-energy estimation: Umbrella sampling, J. Comput. Phys. **23**, 187 (1977).

[35] T. D. Swinburne, P.-W. Ma, and S. L. Dudarev, Low temperature diffusivity of self-interstitial defects in tungsten, New J. Phys. **19**, 073024 (2017).

[36] K. Arakawa, M.-C. Marinica, S. Fitzgerald, L. Proville, D. Nguyen-Manh, S. L. Dudarev, P.-W. Ma, T. D. Swinburne, A. M. Goryaeva, T. Yamada, T. Amino, S. Arai, Y. Yamamoto, K. Higuchi, N. Tanaka, H. Yasuda, T. Yasuda, and H. Mori, Quantum de-trapping and transport of heavy defects in tungsten, Nat. Mater. **19**, 508 (2020).

[37] L. D. Landau and E. M. Lifshitz, *Statistical Physics*, 2nd ed. (Pergamon Press, Oxford, 1969), pp. 174–176.

[38] P.-W. Ma, S. L. Dudarev, and J. S. Wróbel, Dynamic simulation of structural phase transitions in magnetic iron, Phys. Rev. B **96**, 094418 (2017).

[39] P.-W. Ma, S. L. Dudarev, and C. H. Woo, SPILADY: A parallel CPU and GPU code for spin–lattice magnetic molecular dynamics simulations, Comput. Phys. Commun. **207**, 350 (2016).

[40] D. R. Mason, D. Nguyen-Manh, and C. S. Becquart, An empirical potential for simulating vacancy clusters in tungsten, J. Phys.: Condens. Matter **29**, 505501 (2017).

[41] B. N. Dutta and B. Dayal, Lattice constants and thermal expansion of palladium and tungsten up to 878 °C by x-ray method, Phys. Status Solidi (b) **3**, 2253 (1963).

[42] R. Lowrie and A. M. Gonas, Single-crystal elastic properties of tungsten from 24 to 1800 °C, J. Appl. Phys. **38**, 4505 (1967).

[43] R. LeSar, R. Najafabadi, and D. J. Srolovitz, Finite-Temperature Defect Properties from Free-Energy Minimization, Phys. Rev. Lett. **63**, 624 (1989).

[44] J. G. Kirkwood, Statistical mechanics of fluid mixtures, J. Chem. Phys. **3**, 300 (1935).

[45] R. Freitas, M. Asta, and M. de Koning, Nonequilibrium free-energy calculation of solids using LAMMPS, Comput. Mater. Sci. **112**, 333 (2016).

[46] S. Dudarev and A. Sutton, Elastic interactions between nanoscale defects in irradiated materials, Acta Mater. **125**, 425 (2017).

[47] H. Trinkaus, On the investigation of small dislocation loops in cubic crystals by diffuse x-ray scattering, Phys. Status Solidi (b) **54**, 209 (1972).

[48] Please contact PublicationsManager@ukaea.uk.